Next Materials 2 (2024) 100060

Contents lists available at ScienceDirect

Next Materials

journal homepage: www.sciencedirect.com/journal/next-materials

Research article

Design of a composite wound dressing: Combining an electrospun fleece with a free-standing multilayer film

Adrian Hautmann [a], Tobias Hedtke [b], Sonia Sislema-Muñoz [a], Juliana Martins-Schalinski [b], Christian E.H. Schmelzer [b], Thomas Groth [a,c,*]

[a] Department Biomedical Materials, Institute of Pharmacy, Martin Luther University Halle-Wittenberg, Germany
[b] Fraunhofer Institute for Microstructure of Materials and Systems IMWS Halle (Saale), Germany
[c] Interdisciplinary Center for Materials Science, Martin Luther University Halle-Wittenberg, Germany

ARTICLE INFO

Keywords:
Layer-by-Layer
Electrospinning
Wound Dressing
Free-standing Film
Freestanding Membranes

ABSTRACT

Chronic skin wounds place a heavy burden on patients and healthcare systems. To address this problem, we have developed a novel composite material consisting of an electrospun fleece and a free-standing multilayer film that combines the wound healing benefits of both materials. In detail a combination of spray coating and electrospinning is used to create a layer-by-layer film on top of a gelatin fleece, with a final thickness of about 1 mm. A gelatin fleece is partially crosslinked in formaldehyde vapor and 30 pH-sensitive bonding bilayers of partially oxidized hyaluronic acid (HA) and chitosan, followed by 120 bilayers of alginate and chitosan are sprayed on top. The resulting composite is crosslinked with genipin. Uncrosslinked and genipin crosslinked composites are compared to the unprocessed fleece and free-standing multilayer film. The spray coating method produces a stable composite, allows a fast growth of the film part und most importantly retains the nano-topography of the fleece side as confirmed by electron microscopy, profilometry, nano-tomography and dynamic mechanical analysis. To test biocompatibility, cell proliferation experiments with human dermal fibroblasts and THP-1 derived macrophages are performed, proliferative assays are accompanied by immunohistochemical staining and a pro/anti-inflammatory cytokine assay. The composite shows no cytotoxicity and is biocompatible in vitro. Furthermore, the electrospun fibers of the fleece act as a scaffold to highly promote cell adhesion and proliferation, while the modular design of the multilayer free-standing film, in combination with genipin crosslinking, allows the tuning of the anti-inflammatory effect by HA. Overall, the composite seems to be a promising starting point for the design of a novel wound dressing.

1. Introduction

Chronic wounds pose a significant challenge to healthcare systems worldwide, affecting patients' well-being and incurring substantial economic costs. These wounds, which encompass conditions such as diabetic foot ulcers, venous ulcers, and pressure ulcers create a substantial burden on both patients and healthcare providers [1]. Currently, the therapy is characterized by frequent medical interventions, long healing times and long-term continuous treatment with a variety of wound dressings [2]. Acute skin wound healing is characterized by the four dynamic, timely and locally orchestrated processes of hemostasis, inflammation, cell proliferation and tissue remodeling [3]. In contrast, chronic wounds deviate from this normal progression and remain stuck in the inflammatory stage, which does not allow the initiation of the proliferation phase. This chronic inflammation is characterized by elevated protease activity, increased pro-inflammatory cytokines, and reduced levels of growth factors [4]. The impaired angiogenesis leads to insufficient blood supply and therefore lowered oxygenation of the wound bed, perpetuating the inflammation. Similarly, lymphatic vessels are affected in chronic wounds, leading to inadequate drainage of interstitial fluid and a reduced immune response [5]. Furthermore, surveys in the US show that nearly 60% of chronic wounds are associated with microbial infections [6].

Key cell types involved in wound healing are macrophages and fibroblasts. Macrophages, as immune cells, act as 'clean-up' cells, removing debris and bacteria from the wound site in the inflammation phase [7]. In this phase, monocytes are recruited to the wound site, differentiate to macrophages and adopt an activated M1-like phenotype,

* Correspondence to: Department Biomedical Materials, Institute of Pharmacy, Martin Luther University Halle-Wittenberg, 06099 Halle (Saale), Germany.
E-mail address: thomas.groth@pharmazie.uni-halle.de (T. Groth).

https://doi.org/10.1016/j.nxmate.2023.100060
Received 1 July 2023; Received in revised form 9 October 2023; Accepted 31 October 2023
Available online 8 February 2024

driven by pro-inflammatory cytokines, DAMPs (damage-associated molecular patterns) and PAMPs (pathogen-associated molecular patterns)[8]. M1 macrophages exhibit enhanced microbicidal activity by producing reactive oxygen species (ROS) and antimicrobial peptides that contribute to pathogen clearance [4]. They are also capable of engulfing and eliminating foreign particles, debris and apoptotic cells present in the wound area, as well as capturing and displaying foreign antigens, thereby activating the adaptive immune response [9]. Over time, in normal wound healing, external stimuli, for example cytokines secreted by Th2 lymphocytes, contribute to a shift in macrophage activation towards the M2 phenotype [10]. The transition from M1 to M2 macrophages is a dynamic process in wound healing where control of inflammation and tissue repair promotion is essential for the resolution of inflammation and the subsequent phases of wound healing [10]. The M2 activation states include a number of different phenotypes that are associated with regenerative functions. Through their different activation states, macrophages exert regulatory effects on fibroblasts, angiogenesis and wound healing by producing a range of growth factors and cytokines [7]. For example, M1-like macrophages secrete pro-inflammatory interleukin-6 (IL-6), while M2-like macrophages produce interleukin-10 (IL-10), which suppresses the inflammatory response while stimulating fibroblast proliferation and collagen synthesis [7,10]. Fibroblasts migrate to the wound site and secrete collagens, GAGs (glycosaminoglycans), proteoglycans and glycoproteins to form the extracellular matrix that is critical for wound closure [11]. The combined efforts of fibroblasts and macrophages are essential for the regeneration of injured tissue and are the basis for wound contraction and the reepithelization by keratinocytes [7].

To alleviate chronic wounds, conventional wound dressings aim to provide an optimal wound healing environment. Their purposes include the maintenance of a moist healing environment (e.g., films, foams, hydrocolloids, hydrogels), reduction of bacterial load and infection (e.g., dressings containing silver or iodine) or the support of the healing process by collagen, cellulose and other factors [12]. Wound dressings can be produced by a variety of techniques, such as fibrous sheets or fleeces prepared using conventional textile technologies but also electrospinning. Moreover, there are membranes and films prepared by solvent-based techniques or foams by thermal phase inversion techniques [13–15]. A review by Han and Ceilley highlights the limitations of current wound dressing materials, which often address only some of the challenges of chronic wounds and lack active components that promote wound healing through increased activity of tissue cells and neovascularization [16]. Therefore, the complexity of the healing process and the phase dependent requirements of wound dressings have led to the research of active biodegradable scaffolds, which mimic the skin microenvironment [17]. The optimal resolution of chronic wounds requires an integrated approach addressing both the resolution of inflammation and the facilitation of fibroblast migration. One promising strategy might be the combination of composite electrospun scaffolds and free-standing multilayer films prepared by layer-by-layer (LbL) technique to create a controlled microenvironment for wound healing.

Electrospun fibers have gained significant attention as a material for wound dressing applications due to their unique microstructure and mechanical properties [18]. Their small diameter and large surface area provide a suitable environment for cell attachment, proliferation and differentiation, while their high porosity and mechanical strength supports wound healing by providing a supportive scaffold for tissue regeneration [18]. The promoting effect of proteins like collagen, fibrinogen and others implemented into nanofiber matrices on cell attachment and proliferation was proven in several studies [19,20]. Gelatin is a popular biomaterial for electrospinning due to its inherent bioactivity, cytocompatibility, low immunogenicity and ease of processing [21]. Gelatin has been shown to contain functional peptide sequences associated with cell surface receptor integrin binding, the best known being the arginine-glycine-aspartic acid RGD sequence [22]. Electrospun gelatin fleece can serve as a scaffold for fibroblasts, which are responsible for the production of collagen thereby enhancing the formation of granulation tissue and wound closure [23]. A drawback of gelatin is its weak mechanical properties and poor stability in aqueous conditions and against proteolytic enzymes which necessitates a cross-linking step [24].

The LbL technique, based on the complexation of polyelectrolytes on solid surfaces allows the formation of nanometer sized surface coatings but also free-standing films in millimeter scale by the automation of layer deposition [25–27]. Since polysaccharides like alginate, GAGs (e.g. Hyaluronan), and chitosan represent polyelectrolytes they can be used in the LbL process to generate biogenic, biocompatible and even bioactive polyelectrolyte multilayers (PEMs). Such multilayers can have anti-inflammatory, bioactive and anti-bacterial properties dependent on the use of specific polysaccharides [28–31]. Recently, we have demonstrated that such multilayer films can be prepared as free-standing films with a thickness of around 500 μm combined with the incorporation of bioactive factors for controlled release of growth factors, offering potential benefits in chronic wound healing [30]. With the substancial increase of the number of layers, the construction methods of LbL systems becomes increasingly important. Spray coating offers distinctive advantages, as the complexation of the polyelectrolytes is accelerated by the impact of the charged species on the previous layer, instead of relying only on diffusion [32]. Despite yielding thinner free-standing films compared to dip coating, spray coating allows therefore faster complexation and eliminates the need for a rinsing step [32,33]. Alginate (ALG), chitosan (CHI), and hyaluronic acid (HA) have been extensively studied for their wound healing properties and were therefore selected as polyelectrolytes in this study [34,35]. HA and ALG represent polyanions, while CHI, in aqueous solutions with a pH below 6, is a polycation to form PEMs that can control cell adhesion and differentiation [36,37]. ALG, derived from brown seaweed, is a common constituent of hydrogels and can absorb large amounts of wound exudates, creating a moist environment that promotes wound healing [38]. CHI, has a positive charge and can form electrostatic interactions with negatively charged bacteria, helping to prevent infection [39]. HA, a naturally occurring glycosaminoglycan in the body, has a high water-holding capacity which helps to establish a moist wound environment, promoting fibroblasts growth, migration and collagen synthesis, which is important for granulation tissue formation [40]. Most importantly, high molecular weight HA has also anti-inflammatory properties that rely on the binding to the cell receptor CD44, which leads to downregulation of toll-like receptor (TLR) signaling, which in turn mediates NF-κB activation [41,42]. As a result, HA binding to CD44 promotes the release of anti-inflammatory cytokines such as IL-2 and IL-10, switching macrophages to a M2-like state [43]. Due to the presence of ROS (reactive oxygen species) and hyaluronidases in the wound bed, high molecular weight-HA (HMW-HA) gets degraded to low molecular weight-HA (LMW-HA)[5]. Low-HA has been found to promote angiogenesis and lymphangiogenesis, mediated by the LYVE-signaling pathway, contributing to the formation of new blood and lymphatic vessels, which are crucial for wound healing [44]. Due to chemical modifications, it is also used as a popular polymer in controlled drug release systems by retaining its bioactivity [44].

Here, for the first time, PEMs were constructed on an electrospun fleece, by spray coating. The resulting composites attempts to incorporate both biophysical and biochemical cues that should increase cell adhesion, proliferation and anti-inflammatory properties. In particular, we created a composite film consisting of a gelatin-based nanofiber fleece as the basal layer and a thicker multilayer film of HA, CHI and ALG on top. The preserved nano-topography on the cell-facing side is intended to provide topographical cues, while the spray-coated multilayer film with HA provides anti-inflammatory biological cues, has the potential to absorb wound fluid and has antibacterial properties due to the inclusion of CHI and ALG.

2. Methods

2.1. Preparation of composites

2.1.1. Oxidation of hyaluronic acid

Oxidation of HA was conducted according to a protocol published previously [45]. The process is illustrated in Fig. 1. Briefly, 1 g of HA was added slowly into 200 ml dH_2O and stirred overnight. An equivalent of 1 of $NaIO_3$ was then added (0.530 g) and incubated for 24 h in the dark. The product was dialyzed for 3 days against water and lastly freeze dried. The final product was stored at 4 °C for further usage. The oxidation degree was measured by titration and Schiffs test protocols found in above mentioned publication [45].

2.1.2. Fluorescence labelling of chitosan

For an estimated labelling of 20% 100 ml CHI 2 mg/ml solution was mixed with 46 mg fluorescein isothiocyanate (FITC) dissolved in 9 ml of dehydrated methanol and stirred for 3 h in the dark at room temperature. The mixture was precipitated by adding 0.2 M of NaOH until it reached pH 10. The next step was centrifugation at 3500 g for 10 min. Then, the precipitate was washed with methanol three times till there was no fluorescence detected in supernatant. After re-dissolving the precipitate in 30 ml 0.1 M acetic acid the mixture was dialyzed in the dark against distilled water at 4 °C for 3 days. Finally, the mixture was freeze dried for 24 h in the dark.

2.1.3. 6-aminofluorescence labelling of hyaluronic acid

An amount of 200 mg of HA was dissolved in 100 ml 2-(N-morpholino)ethanesulfonic acid (MES) buffer (50 mmol/L, pH 4.75) overnight. Followed by the addition 0.996 mmol of 1-Ethyl-3-(3-dimethylaminopropyl) carbodiimide (EDC) as well as 0.996 mmol of NHS to the solution and a pH adjustment to 7 with sodium hydroxide. For 10% of labelling 17.296 ml of 6-Aminofluorescence (1 mg/ml) solution in dimethyl sulfoxide (DMSO) was added and stirred for 18 h in the dark at room temperature. The product was dialyzed for at least three days until there was no fluorescence detected in the dialysis water. Freeze drying was performed to obtain the final product.

2.1.4. Rhodamine labelling of chitosan

To prepare rhodamine-labelled CHI (CHI-rho), 100 mg of CHI was dissolved in 10 ml of 0.1 M acetic acid, then, 10 ml of methanol and 3.25 ml of 2 mg/ml rhodamine B isothiocyanate (RITC) in methanol were added. The mixture was stirred for 18 h in the dark, followed by purification of the rhodamine-labelled CHI through dialysis. The solution was freeze dried and stored at 4 °C.

2.1.5. Electrospinning

Gelatin was dissolved in acetic acid aqueous solution (50%, v/v) to a final concentration of 20% (w/v). Stirring was necessary to obtain a homogeneous mixture. Electrospinning was performed on a LE-50 electrospinning device (Fluidnatek, Valencia, Spain) equipped with a drum collector and a moving emitter stage. The spinning distance was 180 mm, emitter and collector voltages were set to + 20 kV and − 6 kV, respectively. Fibers were collected on a polypropylene substrate that was fixed to the drum collector. The drum collector was set to 300 rpm. Electrospun gelatin fiber mats with an approximate area of 15 × 30 cm^2 were obtained.

2.1.6. Crosslinking of fleece

A container filled with a volume of 25 ml of a 37% formaldehyde aqueous solution was placed inside a glass desiccator (15.5 cm of diameter and 20 cm height) following an already published protocol [46]. The electrospun gelatin mats were cut to pieces of 5 × 5 cm^2 and incubated in the closed desiccator over a formaldehyde reservoir for 90 min

2.1.7. Spray coating

A 2 mg/ml of CHI solution was prepared by dissolving CHI in 150 mM NaCl solution at 50 °C for 3 h, pH was adjusted to 4 using a 30% acetic acid solution. ALG (5 mg/ml) oxidized hyaluronic acid (oxHA) and HA solution (2 mg/ml) were dissolved in 150 mM NaCl solution, and pH adjusted to 4 using HCl. Afterwards, all solutions were sterilized by filtration using 0.22 μm pore size filters and stored at 4 °C. A vertical spray coater (ND-SP Precision Spray Coater, Nadetech, Spain) was modified to spray horizontally, allowing drainage of excessive polyelectrolyte solution and avoidance of washing steps during layer-by-layer build up. Additionally, a script was written to allow unlimited deposition loops, which was previously limited to 4 bilayers by the proprietary ND-SP spray coater software (2.0.1.0). The electrospun fleece was fixed to the vertical spraying area by a custom 3d printed clamp and for the preparation of free-standing films, a polypropylene substrate was used instead of the fleece. All four syringes were fixed and filled with polyelectrolytes. The first and third syringes with the CHI solution, and the second and forth syringes with the respective polyanion solutions. The first 10 sprayed bilayers contained oxHA and CHI, while the following 20 bilayers, HA and CHI. The subsequent 120 bilayers were made up of ALG and CHI. Regarding the free-standing film, samples were peeled from the polypropylene substrate. The final samples with 150 bilayers were cut into a round shape of 1 cm diameter each, employing a toggle press.

2.1.8. Crosslinking of composites

The cut composites were placed in a 24 well plate and crosslinking started by adding to each well 1 ml of 1 mg/ml Genipin solution prepared in distilled water. The crosslinking reaction took place at 37 °C for 18 h. To stop the reaction the genipin solution was removed, followed by the addition of 70% ethanol for 15 min, which was useful to maintain sterility of the samples. The films were then washed 3 times with sterile PBS for 15 min each under a laminar flow hood.

2.2. Physical studies

2.2.1. Amino acid analysis

To determine the crosslinking degree of fleece, amino acid analysis was performed. Gelatin granulate, formaldehyde-crosslinked and uncrosslinked electrospun gelatin nanofiber fleeces were hydrolyzed in 6 N HCl at 110 °C for 24 h. Free amino acids were subsequently analyzed on a Biochrom 30 amino acid analyzer (Biochrom, UK) according to the standard protocol provided by the manufacturer. For detection and quantification, post-column ninhydrin derivatization was applied with leucine as an external standard.

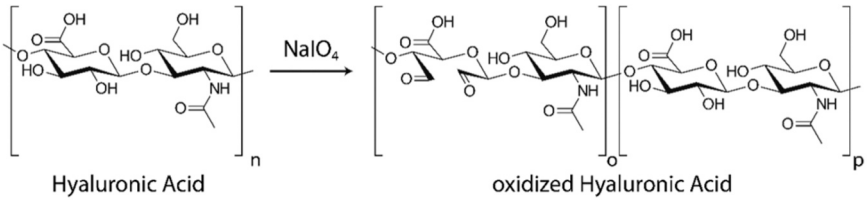

Fig. 1. Introduction of an aldehyde group into HA by sodium-periodate.

2.2.2. Film growth measurements

Confocal laser scanning microscopy (CLSM) was performed with a Carl Zeiss 710 LSM microscope to investigate the film's thickness, swelling and the location of HA-FITC. The samples were prepared according to the described protocol with fluorescence labelled polyelectrolyte solutions and dried in desiccator before observation. The FITC and rhodamine fluorescence was detected using z-stack mode. As for the swelling studies, the dried samples were immersed in PBS after the first observation for 24 h. The microcopy pictures were then extracted with ImageJ (ver. 1.53p), using the 3D object plugin to detect the volume in μm^3 [47]. The volume was divided by the image area to calculate the thickness of respective fluorescent labelled polyelectrolyte.

2.2.3. Profilometry

Optical profilometric analyses were performed using a laser-scanning microscope (VK-X1050, Keyence) to determine the thickness. The wet samples were placed on a slide and a part of the sample was cut with a razor blade to obtain a smooth edge for height measurement. The analysis was performed with a red laser at 661 nm in reflection mode.

2.2.4. Environmental scanning electron microscope

The samples were cut from each specimen into smaller pieces of approximately $2 \times 2\ mm^2$ and placed on self-adhesive conductive carbon tape (Plano GmbH, Wetzlar, Germany) on microscope stubs. Afterwards the samples were then coated with a thin layer of platinum (2–3 nm) and analyzed on a Quanta 3D Field-Emission Gun Scanning Electron Microscope (FEG-SEM) (FEI, Hillsboro, OR, USA) at an acceleration voltage of 5 kV.

2.2.5. Nano-computed tomography

Imaging experiments were performed on dried samples of the composite materials in a Carl Zeiss Xradia 810 Ultra X-ray microscope (XRM) equipped with a chromium source (5.4 keV). A small piece of each sample was glued onto the tip of a metallic pin that was inserted in the sample holder of the microscope. The imaging experiments were performed using Zernike phase-contrast, a field-of-view of 64 μm^2 and a total of 1001 projection images were acquired by rotating the sample over 180°. The exposure time for each projection was 20 s and a detector binning of 2×2 was used, resulting in an isotropic voxel size of 128 nm in the final image. Image reconstruction was performed by a filtered back-projection algorithm using the XMReconstructor software integrated into the microscope. The tomograms obtained were then exported as a stack of 16-bit TIFF images and visualized in 3D using Avizo (Thermo Fischer, version 3D 2022.2). Image processing and segmentation were done in the same program, by first applying a median filter followed by segmenting the sample using an interactive threshold. Fiber tracing was done using an auto skeleton module, porosity was estimated by the volume fraction module, and fiber diameter by the spatial graph statistics module. Considering resolution, only values larger than 3 pixels were considered in the fiber diameter distribution.

2.2.6. Dynamic mechanical analysis

A TA.XTplusC from Stable Micro Systems (Godalming, UK) was used to determine mechanical properties using the penetrating ball method. Samples were fixed over a perforated metal plate. A 5 mm diameter spherical ball probe was pressed into the surface at a constant speed of 1 mm/s and the force-displacement relationship was recorded after reaching a trigger force of 0.005 N. The sampling rate was set to 200 measurements per second and the test was terminated when the material failed. The ultimate tensile strength was calculated by dividing the force applied at the failure point by the area in contact with the sample. For determination of the Young's modulus the initial linear slope between 1% and 4% of the stress/strain curve was used.

2.3. Biological studies

2.3.1. Cell culture

In this study human dermal fibroblast (HDF) and THP-1 human monocytes were used. The HDF were grown in Dulbecco's modified Eagle medium (DMEM without pyruvate, with 4.5 g/L glucose) (Carl Roth) and THP-1 in RPMI1640 (with L-Glutamine) (Lonza), both supplemented with 10% fetal bovine serum (FBS, Biochrom AG, Berlin, Germany) and antibiotic–antimycotic solution (AAS, Lonza, Wuppertal, Germany) at 37 °C in a humidified 5% CO_2 using a NUAIRE DH Autoflow incubator (NuAire Corp, Plymouth, MN, USA). Cells were cultured in T75 cell culture flasks and media was changed every second day; cell subculturing was performed to maintain cell density from 5×10^5 to 5×10^6 cell per ml. HDF cells were harvested with 0.25% trypsin/0.02% ethylenediaminetetraacetic acid (EDTA) solution at 37 °C for 3–5 min. The trypsin reaction was stopped by adding DMEM with 10% FBS. Subsequently, the cells were re-suspended and seeded at a desired density on the well plate. The THP-1 cells were differentiated with 200 nM phorbol-12-myristate-13-acetate (PMA) to M0-like macrophages following a published procedure [42]. Afterwards cells were harvested with 0.25% trypsin/0.02% EDTA solution at 37 °C for 3 min and the help of a cell scraper.

2.3.2. Biocompatibility studies

All samples were sterilized by immersion in 70% ethanol, with subsequent threefold washing with PBS for 5 min each. A cell suspension with a density of 25,000 cells per well was seeded in a 24 well plate and incubated for 12 h. After a media change composites and films were carefully added on top of the cells after the latter were attached to the well bottom following a previous published protocol [30]. Cell damage was avoided as the films float over the cell layer. After 24 h the films were temporarily transferred to a new well plate. Then samples were removed before each measurement, to avoid effects of cell adhesion to the samples. The metabolic activity of NHDF cells cultured exposed to the composites and films were analyzed using a resazurin based assay (Deep Blue Cell Viability Kit (BioLegend, San Diego, USA)). Deep Blue was prepared at a ratio of 1:10 with colorless DMEM (without pyruvate, with 4.5 g/L glucose (Lonza, Basel, Switzerland)), added to each well and incubated at 37 °C for 3 h. After incubation, duplicates of 100 µl of the supernatant were transferred to a black 96-well-plate (Greiner Bio-One International GmbH). The converted fluorescent products were photometrically quantified at an excitation wavelength of 544 nm and an emission wavelength of 590 nm using a plate reader (FLUOstar, BMG LabTech, Offenburg, Germany). Cells without samples were used as negative control. After measurements were conducted, the DeepBlue medium was aspirated from the wells and was replaced by DMEM medium. The films, which were stored in a different well plate, were added back to the initial wells plate. The same procedure was repeated on day 3 and day 7.

2.3.3. Live/Dead cell assay

HDF Cells (50,000 cells/well) were incubated for 7 days on top of the samples. Medium change was undertaken every 3 days. Z-Stacks of Samples were recording using a Carl Zeiss ZEN 710 LSM after day 7. Z-stacks were necessary since the samples possess a macroscopically rough surface. A max-intensity projection process was undertaken with ZEN 2012 (v.8.1) to add up all signals present on all slices of the z-stack. Topro3 (Thermo Fisher Scientific, Germany) was used to stain any present DNA content, which allows the location of nuclei. CellTracker Green CMFDA (Thermo Fisher Scientific, Germany), which is only contained in the cell by metabolically active cells, was used to stain living cells. With ImageJ (ver. 1.53p) the number of nuclei was determined by thresholding and particle analysis. Afterwards a cell mask was created using the tresholded CellTracker Green CMFDA channel. Finally, the ImageJ image calculator was used to subtract the cell mask from the nucleus mask. Any remaining particles (stained DNA without Co-

Localization of a living cell) were considered dead cells.

2.3.4. Pro- and anti-inflammatory cytokine production assay

To assess the potential anti-inflammatory activity of the composites, the concentration of Interleukin 6 and 10 secreted by THP-1 derived macrophages was assessed by the enzyme-linked immunosorbent assay (ELISA). Previously sterilized, native composites, genipin crosslinked composites and fleece were placed into two 24-well tissue culture plates and fixed in place by glass cloning rings. Then, 250,000 THP-1 derived macrophages were seeded on top of each sample, and in empty wells as control sample. After 24 h incubation at 37 °C, 5% CO_2 in humidified air, the supernatant was collected from each well and kept in low protein binding tubes (Protein LoBind, Eppendorf, Germany) at − 80 °C for further analysis. Both plates with samples were threefold washed with PBS. To one plate 500 µl of fresh media was added, while to the second plate 500 µl media containing lipopolysaccharides (LPS) at a concentration of 1 µg/ml, similarly, to above mentioned conditions after 24 h incubation the supernatant was collected and kept at − 80 °C. Afterwards, plates were washed with PBS and samples were transferred to fresh well plates for cell viability assay, as previously described, by resazurin based DeepBlue Assay. Collected supernatant from first and second day of culturing were analyzed to detect the pro-inflammatory cytokine IL-6 and anti-inflammatory cytokine IL-10. Assays were conducted according to manufacturer instructions for Human IL-6 and Human IL-10 with the standard ABTS ELISA development kit (Peprotech, USA). Color development was monitored each 5 min with an ELISA plate reader at 405 nm and wavelength correction at 620 nm, during 30 and 40 min respectively.

2.3.5. Statistical testing

Quantitative data was statistically processed using OriginPro 2019 (v.9.6.0.172, OriginLab Corporation, Northampton, USA). Normally distribution was verified by Shapiro-Wilk. Subsequently, one-way analysis of variance (ANOVA) with a post-hoc Tukey test was used. Nonparametric data were tested with a Kruskal-Wallis test. The data is represented as mean values ± standard deviations (SD). Statistical significance is shown by asterisks in the figures ($p \leq 0.05$).

3. Results and discussion

3.1. Physical studies

3.1.1. Fleece characterization

Electrospun nanofiber fleeces can provide nano-topography that greatly improves cell adhesion and growth. However, gelatin-based fleeces lack stability in aqueous media and face proteolytic degradation in a physiological environment [21]. Since the subsequent spray coating process relies on polyelectrolytes dissolved in water, the fleeces were crosslinked with formaldehyde vapor before further processing. Formaldehyde introduces covalent crosslinks in the protein fleece that stabilize the fibrous structure. Crosslinking in liquid phase would alter the microstructure due to fiber swelling. An amino acid analysis confirmed a reduced amount of the amino acids lysine and tyrosine, which are involved in formaldehyde-mediated crosslinking (Fig. 2**A**). The detectable amount of free lysine after crosslinking decreased by 10%. No free tyrosine was detectable after formaldehyde treatment. The topography of the crosslinked electrospun elastin/gelatin nanofibrous fleece was analyzed by nanoscale X-ray computed tomography (nano-CT) using Zernike phase contrast. A smooth fiber structure can be confirmed throughout the whole fleece (Fig. 2**B**). The mean fiber diameter after crosslinking was 0.28 µm ± 0.08 µm as shown in Fig. 2**C**, a representation of the microstructure. The porosity was calculated from the nano-CT data to be 75%. Both fiber diameter and porosity are known to stimulate fibroblast growth in this range [48].

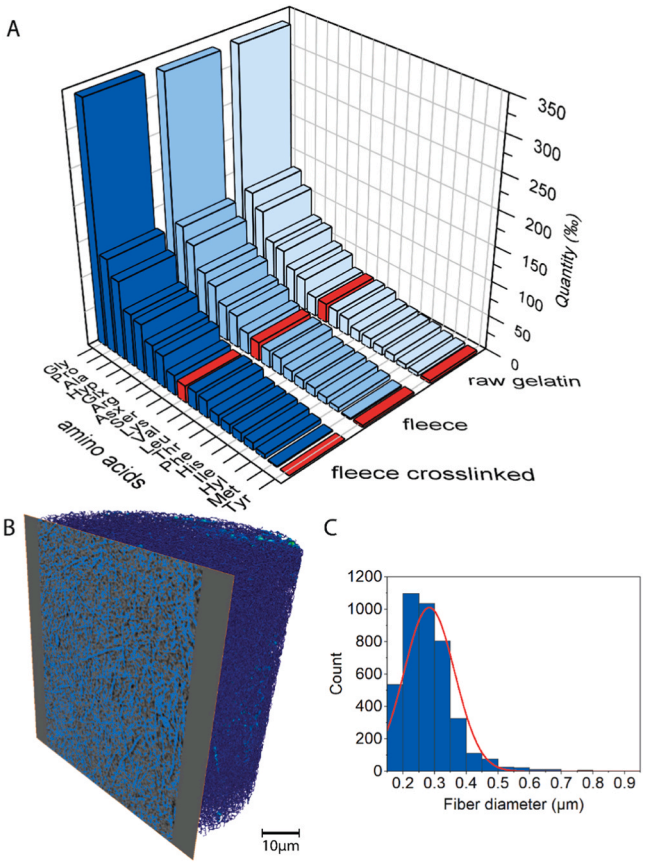

Fig. 2. A) Amino acid analysis. In red are the quantities of the primary amine-containing amino acids lysine and tyrosine marked. These are noticeably decreased between the uncrosslinked and crosslinked fleece. **B)** Nano-CT image of fleece representing the microstructure of the electrospun formaldehyde crosslinked gelatin fleece. **C)** Fiber diameter distribution of the electrospun elastin/gelatin fleece after chemical crosslinking with formaldehyde vapor.

3.1.2. Composite architecture

Spray coating has been shown to be a superior method compared to dip coating in LbL assembly, as it allows for faster deposition of the polyelectrolytes, and eliminates the need for washing, provided sufficient drainage is achieved [32]. By modifying the spray coater to spray horizontally, we could reduce the time for the preparation of one layer on an area of 15 × 15 cm to 1.6 mins. Additionally, the crosslinking of the electrospun fleece was important to guarantee stability of this substrate during the full duration of the spray coating process, where large quantities of aqueous solutions were used. To functionalize the composite and improve its stability, a complex film architecture was selected; The first 10 bilayers were comprised of alternating oxHA and CHI, while the next 20 bilayers of HA/CHI, the final 120 bilayers consisted of ALG/CHI (as shown in Fig. 3).

The purpose of the first 10 bilayers was to enhance the bonding between the layers and the electrospun fleece, by utilizing oxHA, which allows crosslinking of amine groups by imine bond formation [48,49]. The successful oxidation was confirmed by Schiff reaction. A degree of substitution of 20.85 ± 1.1% was measured, indicating a comparable degree of substitution to earlier studies employing oxHA for PEMs. [49]. The next 20 bilayers were made up of native HA and CHI to exploit the anti-inflammatory effects of HA [12]. The final 120 bilayers of ALG/CHI were added because the layer thickness increases much faster than with HA/CHI. Furthermore, the excellent swelling properties of alginate could be exploited for wound dressing applications.

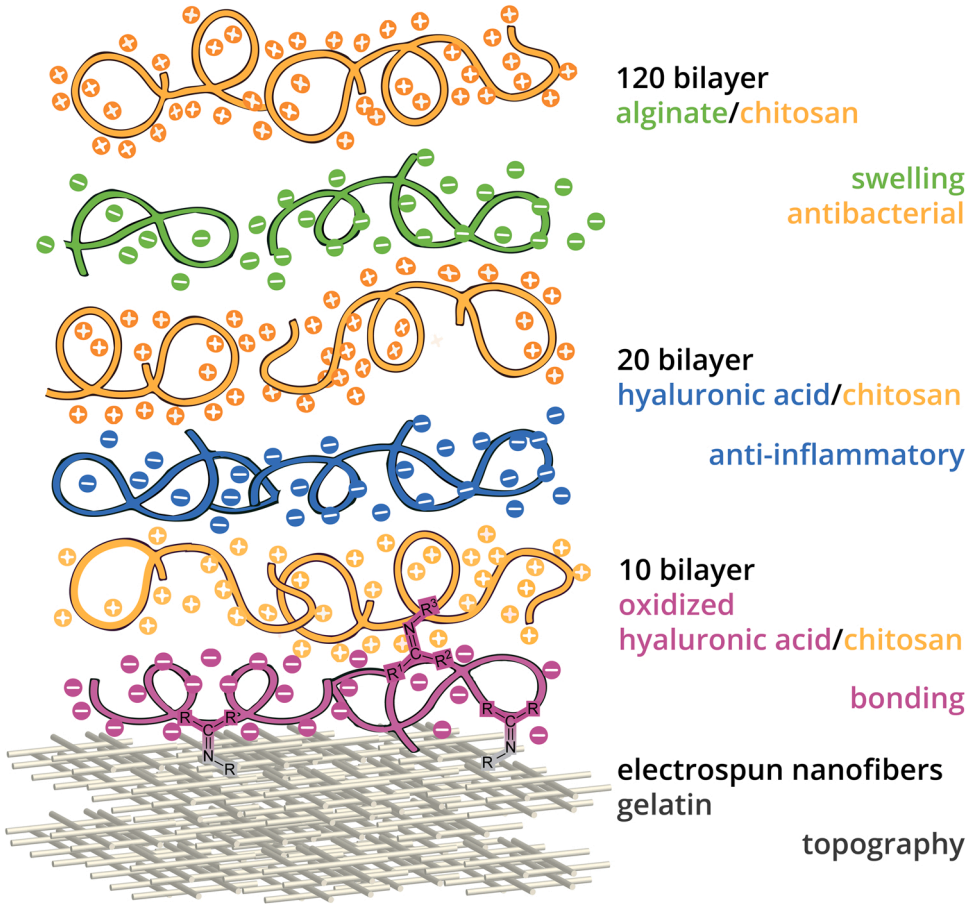

Fig. 3. Composite architecture with a total number of 150 bilayers. Polymer pairs represent bilayer combination with their respective number. Right justified their intended function is given.

3.1.3. *Film growth on fleece*

To determine the thickness of the film at various time points during deposition, we used fluorescence-labeled CHI and quantified it using z-stacks recorded by confocal laser scanning microscopy (CLSM).

The results (Fig. 4**A**) show that the first 30 bilayers, composed of oxHA/CHI and HA/CHI, exhibited a moderate increase in thickness, suggesting a linear deposition process in which the polyelectrolytes interact only with polyelectrolytes of opposite charge to form the next layer of the film. The addition of ALG/CHI as layer pair, resulted in an exponential increase in thickness. This exponential growth is attributed to the diffusion of at least one of the polyelectrolytes throughout the multilayers/film, leading to the restructuring of the film with more hydrogel-like properties [50]. In particular for CHI/ALG bilayers a fast thickness growth is reported, caused by the high charge density of ALG [51]. However, after around 100 bilayers, the rate of thickness growth slowed down again. As previously described in the literature, there

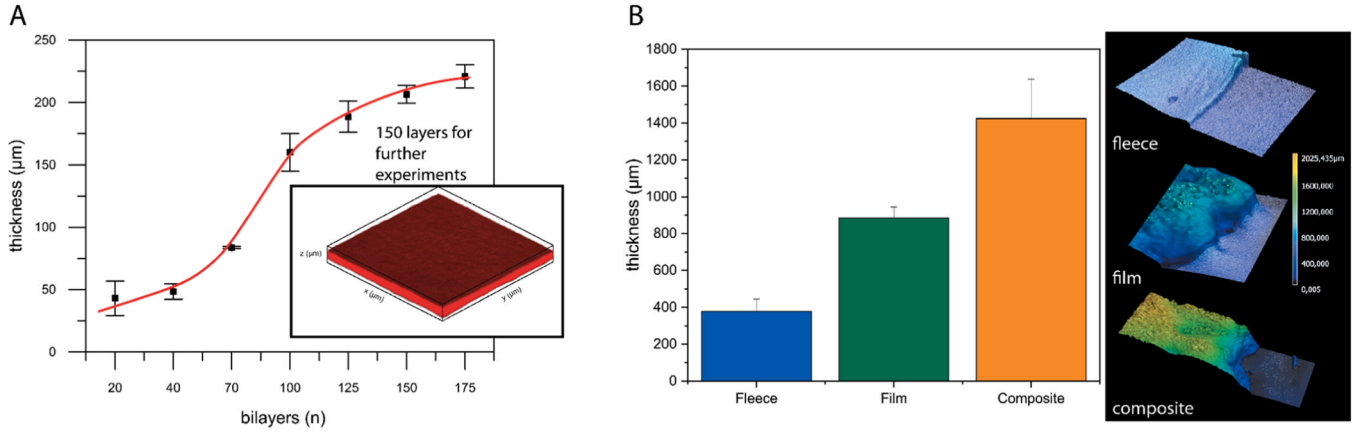

Fig. 4. A) Thickness growth of the free-standing film (without fleece), CHI-rhodamine was used in layer build up. The thickness was derived from the volume of apparent fluorescence found in CLSM z-stacks. The films showed a linear-exponential-linear growth (sigmoidal fitting (Boltzmann) adj. $R^2 = 0.997 \pm 0.01$). 150 bilayers were chosen for further experiments. $n \geq 5$ **B)** Optical Profilometry images of wet fleece, film, and composites. Differences between the sum of the thickness of fleece + film on one hand and the composite on the other, indicate a partly diffusion of components. $n \geq 5$, all sig. to each other $^*p \leq 0.05$.

comes a point during the formation of PEMs where exponential growth switches back to linear growth [51]. Triggered by decreased effect of ion pairing and coulomb forces towards multilayer formation [52]. However, the combined use of different polyelectrolytes limits a comprehensive understanding of the growth mechanism. Nonetheless, the partly exponential growth of the ALG/CHI allows for the efficient and cost-effective production of the free-standing film/film part of the composite to achieve a thickness required for a potential application as wound dressing. 150 bilayers were selected as the optimal balance between preparation time and resulting thickness.

3.1.4. *Structural characterization of composite*

Fig. 4**B** depicts the thickness of the wet composites measured by profilometry. It is evident that most of the composite is comprised of the film, with only about a third being constituted by the fleece. Since the total thickness of the composite is smaller than the sum of the thickness of each individual component, penetration, and successful bonding of bilayers into the fleece is presumable. Although the polyelectrolyte solution is sprayed with a droplet size of well below 1 µm, the LbL-system can bridge 5–10 µm gaps between the fibers (Fig. 5). Here the fiber network might function as an electrostatic barrier through its interfacial interactions, as a result fiber spanning occurs across the larger pores as the LbL cycle is repeated [53]. However, the film does not penetrate or diffuse through the whole composite as the penetration is limited to less than 100 µm inside of the fleece (Fig. 4**B**). Therefore, the topography of the bottom side is still intact, which was also confirmed by nano-CT

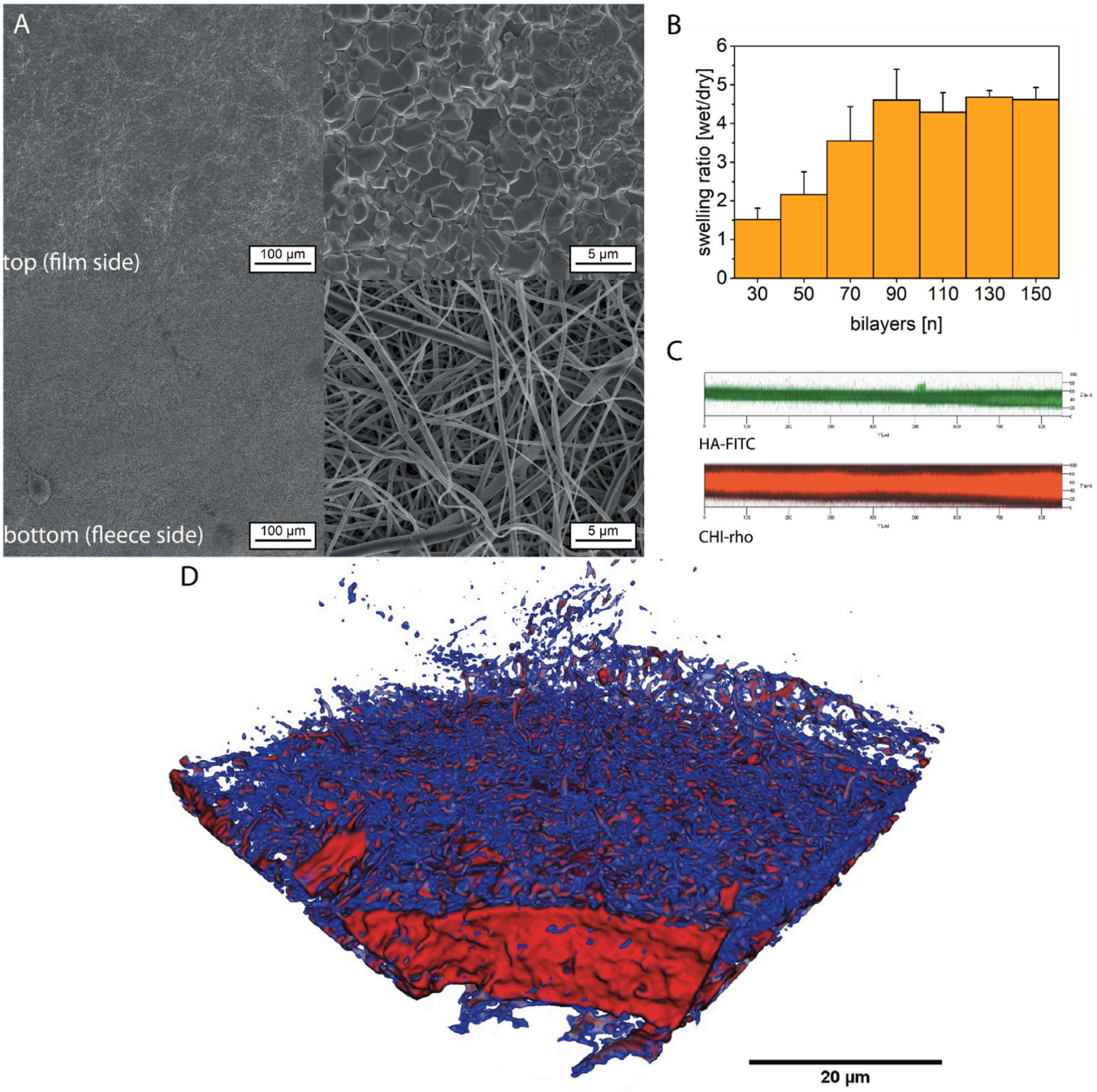

Fig. 5. A) ESEM images of dry composites. **B)** Swelling ratio of the film at several layer numbers determined by CLSM based on the fluorescence distribution of CHI-FITC, constitutes the polycation for all bilayers. n = 5 **C)** Location of HA determined by fluorescent HA-FITC inside the CHI-rho detected by CLSM-based z-stacks. HA-FITC appears to diffuse to a certain degree throughout the multilayer film **D)** Nano-CT image of the native composite (flipped; fibers on top (blue), film below (red)).

image in Fig. 5**D**, where the different densities of the two components are identifiable. In this way polyelectrolyte multilayers form an effective barrier against the environment to prevent for example penetration of bacteria from the outer environment, demonstrating the unique asymmetric properties of this composite. Fig. 5**C** depicts a cross section of the film as CLSM z-stack (CHI-rho channel). HA-FITC used as a polyelectrolyte in the PEMs remained mostly at the bottom of the film part, indicating a limited diffusion.

3.1.5. *Swelling, dynamic mechanical analysis and hydrophilicity*

Swelling of the composite was determined by CLSM using CHI-FITC as a fluorescence tracer in the film (Fig. 5B). The samples were dried for 3 days, measured and re-submerged prior to the second measurement. The first 30 bilayers are composed of CHI/(ox)HA, while the consecutive 110 bilayers are made of CHI/ALG, which is known to have superior swelling properties. The swelling ratio increases with the number of bilayers and plateaued at 90 bilayers. The first 30 bilayers are composed of CHI/(ox)HA, while the consecutive 110 bilayers are made of CHI/ALG.- ALG/CHI are known to have superior swelling properties [30]. With increasing number of layers, the percentage share of the ALG/CHI bilayers increases, while the influence of the CHI/oxHA layers decreases. These show less swelling ability rooted in the effect of oxHA crosslinking by imine bonds between HA and CHI, which reduces the amount of hydrophilic amine groups and the mobility of the polyelectrolytes [54].

The Young's modulus and tensile strength of composites used in wound healing is of particular interest, as sufficient mechanical stability is key for covering a wound and protect it from the environment, while allowing flexibility for the user. To estimate the Young's modulus, the samples were studied with a texture analyzer using a ball penetration test to measure the elongation of the material at an increasing force. As shown in Fig. 6, there is no significant increase in tensile strength or Young's modulus when the film was fabricated on top of the fleece to form the composite. The composite, with the fleece below and the free-standing film on top, can be a considered a two-component system. The fleece is the less elastic, more rigid component in this system. Therefore, the Young's modulus is also a result of the two-component system. Here, the Young's modulus is representative for the properties of the film rather than the fleece since it is the first to contact the probe due to the penetrating ball method. As the Young's modulus is calculated from the initial elastic deformation, it is characterizing the elastic properties of the film in this assay. As a result, the Young's modulus is lower for the composite. In a comparable manner, the tensile strength is also dependent mainly on the fleece. Hence the free-standing film, which is more hydrogel-like in the wet state, has no significant influence. The additional genipin crosslinking of the composite did not lead to a significant increase in either of the two properties. Probably, the crosslinking degree could be increased, or a more sensitive test method used. For an application as a wound dressing, the tensile strength must be improved. However, the composites show comparable tensile strength as alginate dressings (e.g., Kaltostat® 1.3 ± 0.2 MPa), which are usually combined with a secondary wound dressing [55].

However, the crosslinking of the composite by genipin results in a slight modification of the fleece surface. This can be seen in the captive bubble contact angle measurement, where the drop shape of an air bubble which is in contact with the surface of the fleece is analyzed (Fig. 6**C**). The result indicates a less hydrophilic state, as genipin crosslinks free amine groups, providing aromatic heterocyclic ring systems, which decrease the hydration of the polymer [26]. Although it must be noted that the contact angle cannot be compared to flat surfaces, since it is an apparent contact angle, dependent on the roughness of the surface.

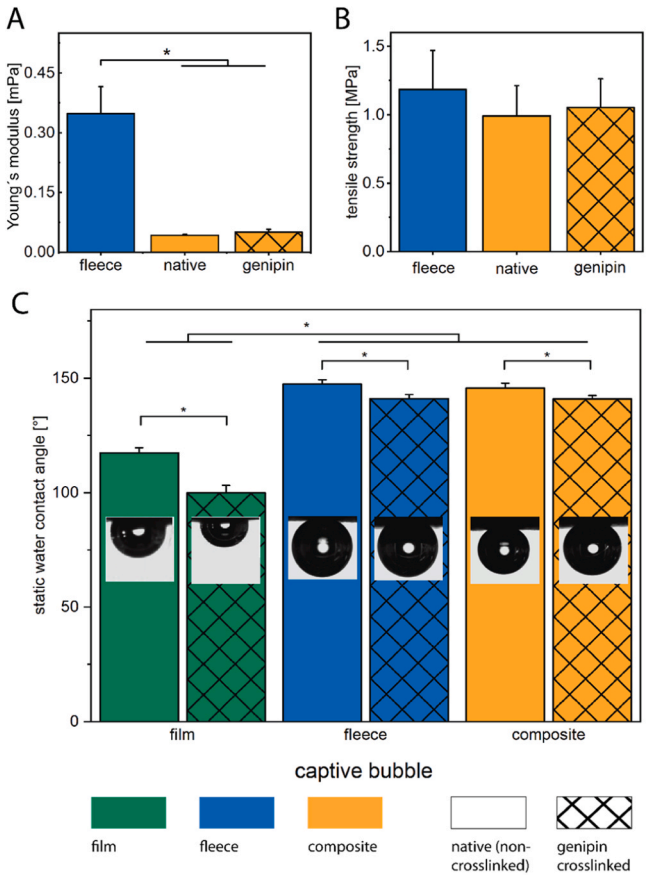

Fig. 6. A) Young's modulus and **B)** Tensile strength of wetted samples, determined by using a ball penetration test. Original stress/strain curves can be found in **S1**. $n \geq 3$ **C)** Contact angle measurement by the captive bubble method. Higher values indicate a less hydrophilic nature. $n \geq 5$.

3.2. *Biological characterization*

3.2.1. *Cytotoxicity and cell growth of fibroblasts*

The cytotoxicity of the individual components and the composite was analyzed by evaluating the cell growth of human dermal fibroblasts underneath the samples (Fig. 7**A**). After 1, 3 and 7 days the cell viability was tested using the resazurin based DeepBlue assay to test if any cytotoxic components diffuse out of the samples and negatively influence cell growth on the well bottom. As shown in Fig. 7, after day 1 and day 3 neither film, fleece nor the composite showed any toxic effect towards the cells or any significant differences in cell viability. After day 7, measured cell viability is significantly higher in the composite and film samples, regardless of crosslinking. Most probably this is a result of an increase of cell growth by the effect of HA [40]. Additionally, there could be a buffering effect of the swollen films, which are able to store mitogenic serum components or growth factors released from cells. These components could be released afterwards, increasing cell growth [30].

Another cell growth and live/dead assay was performed by seeding cells on top of the samples (Fig. 7**B** and Fig. 8). The composite samples were therefore flipped so that the fleece side was facing upwards. The genipin crosslinked composite allowed significantly more cell growth from day 1 to day 3 compared to the control and the films. While the fleece samples showed comparable cell growth, with prolonged contact with the media, the fleece began to shrink and collapse, resulting in a

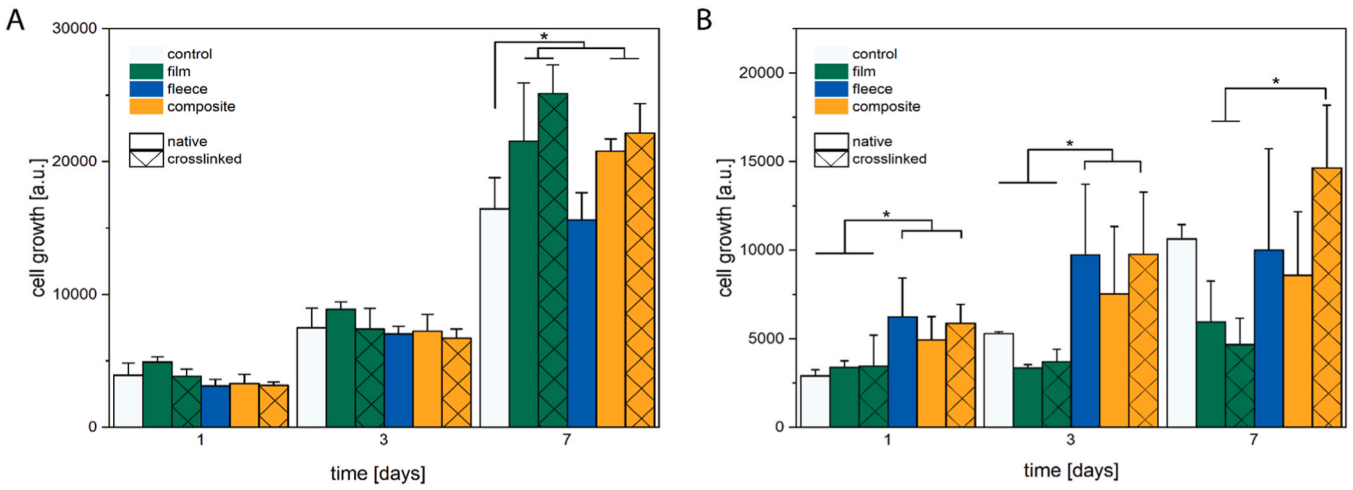

Fig. 7. **A)** Cell growth assay of with HDF cells seeded on the well plate's bottom underneath the samples. All samples show no significant difference to the control (cells cultured on TCPS). **B)** Cell growth assay with HDF cells cultured on top of the samples. Both assays based on DeepBlue assay. (n = 5).

decreased cell growth and increased standard deviation at day 7 compared to day 3. The native and crosslinked composite remained stable throughout the 7-day period. However, cell growth was not significantly higher after 7 days compared to the TCPS control. The film samples demonstrated low cell growth due the low stiffness of the surface of free-standing multilayer films and high hydrophilicity of the surface, resulting in marginal cell adhesion and only small increases in cell growth on days 3 and 7 as shown previously in a comparable study [26].

Films and fleece were excluded from further HDF studies due to poor cell growth. Live/dead cell ratios after 7 days were assessed using a CLSM-based assay recording cell area and nuclei (Fig. 8). Z-stacks of the 3d topography and incorporated cells were recorded and flattened with maximum intensity projection. Nuclei, without association of a cytoplasm were counted as dead cells, cytoplasm without associated nuclei were not considered as adherent cells. Genipin crosslinked samples had the highest cell counts, followed by the native composite and the control. However, the genipin composite had a slightly higher percentage of dead cells. The results indicate that cells can adhere to the gelatin scaffolds, regardless of genipin crosslinking. The increased cell number in the genipin crosslinked samples may be attributed to the reduced hydrophilicity (Fig. 6), which is known to enhance protein adsorption [56]. As a result of the adsorption of proteins like cell secreted fibronectin, cell adhesion is increased [57]. Altogether, the fleece increased cell growth by providing a larger attachment area and possibly by the presentation of RGD sequences in gelatin for integrin-mediated cell binding [22].

3.2.2. *Inflammatory response of macrophages*

Macrophages play a crucial role in induction and resolution of inflammation, key processes in wound healing [8]. In this study, M0 activated macrophages derived from THP-1 cells were used. Cell viability assays were performed after seeding macrophages onto the fleece side of the composite for 48 h (Fig. 9). Compared to the TCPS control, macrophage viability and corresponding quantity of cells on the samples was significantly lower, although the fleece part of the composite should provide necessary cues for macrophage adhesion. The genipin crosslinking did increase cell adhesion comparable to the effect seen at the cell growth assay with HDF cells.

Production of pro- and anti-inflammatory cytokines (IL-6 and IL-10) by macrophages was studied with and without stimulation of cells by LPS as done in a previous study of our group [58]. IL-6 is a pro-inflammatory cytokine produced mainly by M1 activated macrophages and acts in an autocrine and paracrine manner to modulate various cellular processes, including inflammation, immune response and cell proliferation [59]. IL-10 on the other hand is commonly associated with M2 polarized macrophages, characterized as a mostly anti-inflammatory phenotype [10]. As a result, the IL-6 and IL-10 secretion can be used as a marker for macrophage differentiation [60]. Biomaterials are able to modulate these activation modes of macrophages by a number of direct and indirect factors like topography, hydrophobicity and surface chemistry [61]. According to the data presented in Fig. 9**B**, non LPS stimulated macrophages cultured on both native and genipin crosslinked composites for 48 h show a higher release of IL-10 compared to the fleece, indicating an M2-like state. This observation suggests that the topographical adhesion cues may play a role, which are known to nudge cells to an M2 pro healing phenotype [59]. Furthermore, HMW-HA, as used in this study, is known to have the ability to increase IL-10 secretion. This effect is attributed to the ability of HMW-HA to counteract the effects of LMW-HA on TLR mediated activation by inhibiting the NF-κB pathway [9,41,62]. As a result, HMW-HA can promote macrophage differentiation from M1 to M2 [63].

IL-6 production can be stimulated by a variety of factors, including microbial components and damage-associated molecules, like LPS, via the NF-κB pathway [64]. Our results show a decrease in the M1-relevant IL-6 expression in LPS-stimulated cells seeded on all composites in comparison to the fleece. Our findings suggest that HA modulates the IL-6 production, by downregulating NF-κB activation through ligation of CD44 [65]. Since the fleece part of the composites is not coated by the PEMs (Fig. 5) we expect no direct surface mediation of CD44-receptor by HA. More likely is the diffusion of HA molecules through the fleece to the macrophages where they can associate with the cell receptors. We hypothesize that the high release of IL-6 by the cells seeded on the fleece is caused by the crosslinking of the fleece by formaldehyde vapor before the spray coating. This effect could be counteracted by the influence of HA in the composite samples or by use of another crosslinking method in future studies. Overall, the combination of topographical cues provided by the composite materials and the influence of HMW-HA on the activation state of macrophages likely contributes to the promotion of an M2-like phenotype and enhanced secretion of IL-10 as well as downregulating the IL-6 secretion in macrophages cultured on the native and genipin crosslinked composites. As a result, the composite could have a significant effect on resolving inflammation and promoting tissue repair.

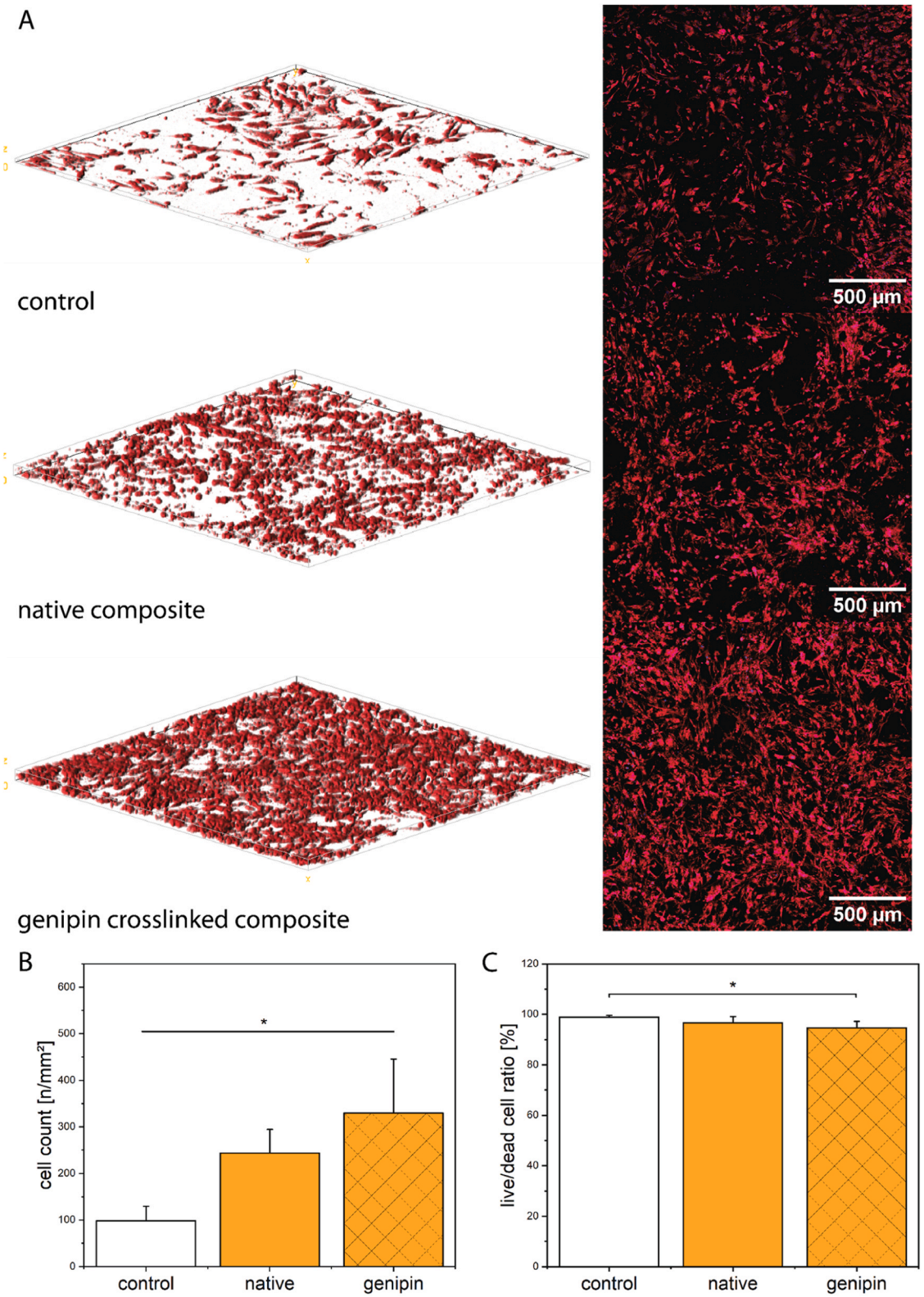

Fig. 8. A) NHDF cells cultured for 7 days on top of the samples. Control on TCPS. In **S2** the original live/dead images can be found. **B)** Quantitative data, determined by z-stack maximum intensity projection and automated counting. The number of cells in each sample are significant to each other. $n \geq 6$ **C)** Live/dead cell ratio, all nuclei without associated cell body were considered as dead. Genipin crosslinked composites lead to a significant lower live/dead cell ratio compared to the control. $n \geq 6$.

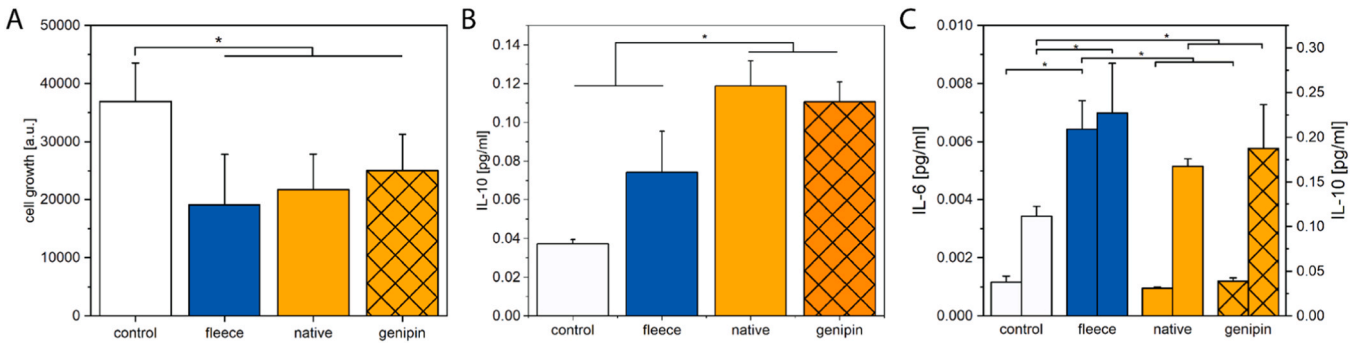

Fig. 9. A) cell growth of THP-1 derived macrophages without LPS stimulation. n ≥ 5 **B)** IL-10 secretion of THP-1 derived macrophages normalized to cell growth **without LPS** after 48 h. IL-6 secretion was not detectable without LPS stimulation n ≥ 3 **C)** Interleukin ratio IL-6 (left) and IL-10 (right) normalized to cell growth **with LPS** after 48 h. n ≥ 3.

4. Conclusion

The presented modified spray coating process is able to add a multilayer system efficiently on top of the fleece part. The result is a novel composite which provides nano-topography, while the free-standing multilayer film part shows excellent swelling properties and incorporates HA for anti-inflammatory effect. Moreover, it greatly improves cell adhesion and growth of fibroblasts, which is novel for free-standing multilayer films, as they usually lack topography, have low stiffness and high hydrophilicity. The nano fleece counteracts this by acting as a scaffold to enable fibroblast migration and adhesion, while the modular design of the free-standing multilayer film allows control and tuning of key properties, specially, stability and swelling, which are necessary for the design of wound dressings. The use of HA and CHI as bioactive components of the film part introduces anti-inflammatory, anti-bacterial and wound healing capabilities. Genipin crosslinking of the composite enhances the composites bioactive properties while there is no difference in the inflammatory response. In the future this composite can be tailored to different sizes and shapes and produced by continuous spray coating processes. In addition, due to the layered nature of the system, this composite has the potential to incorporate a wide range of other polyelectrolytes, drugs, growth factors or carriers, such as charged nanoparticles or lipoplexes, and can be designed asymmetrically to control cell adhesion for other medical applications. In conclusion our study presents for the first time a successful combination of a nano fleece with a free-standing multilayer film for wound healing applications. Overall, this composite shows great promise as a platform for the development of novel bioactive wound dressings.

Declaration of Competing Interest

The authors declare that they have no known competing financial interests or personal relationships that could have appeared to influence the work reported in this paper.

Acknowledgements

Prof. Jürgen Brickmann and Heiko Steenbock (University of Lübeck) are thanked for assistance with amino acid analysis. Zahra Damayanti (Martin Luther University Halle-Wittenberg) is thanked for conducting experiments on oxidation, spray coating and film growth measurements. Marko Stäter (Fraunhofer IMWS) is thanked for assistance with mechanical testing and electron microscopy. Maria Morawietz and Sandra Saremba (Fraunhofer IMWS) are thanked for assistance with optical profilometry. The work was supported by the European Regional Development Fund in Saxony-Anhalt (project ProTect), by the Fraunhofer Internal programs under Grant No.: Attract 069-608203 (CEHS) and the Federal Ministry of Education and Research under the GO-Bio initial project “Active Layers” (16LW0046).

Appendix A. Supporting information

Supplementary data associated with this article can be found in the online version at doi:10.1016/j.nxmate.2023.100060.

References

[1] G.S. Lazarus, D.M. Cooper, D.R. Knighton, R.E. Percoraro, G. Rodeheaver, M. C. Robson, Definitions and guidelines for assessment of wounds and evaluation of healing, Wound Repair Regen. Off. Publ. Wound Heal. Soc. Eur. Tissue Repair Soc. 2 (1994) 165–170, https://doi.org/10.1046/j.1524-475X.1994.20305.x.
[2] E. Eriksson, P.Y. Liu, G.S. Schultz, M.M. Martins-Green, R. Tanaka, D. Weir, L. J. Gould, D.G. Armstrong, G.W. Gibbons, R. Wolcott, O.O. Olutoye, R.S. Kirsner, G. C. Gurtner, Chronic wounds: Treatment consensus, Wound Repair Regen. Off. Publ. Wound Heal. Soc. and Eur. Tissue Repair Soc. 30 (2022) 156–171, https://doi.org/10.1111/wrr.12994.
[3] C.K. Sen, Human wound and its burden: updated 2020 compendium of estimates, Adv. Wound care 10 (2021) 281–292, https://doi.org/10.1089/wound.2021.0026.
[4] L. Cañedo-Dorantes, M. Cañedo-Ayala, Skin acute wound healing: a comprehensive review, Int. J. Inflamm. 2019 (2019) 3706315, https://doi.org/10.1155/2019/3706315.
[5] A.P. Veith, K. Henderson, A. Spencer, A.D. Sligar, A.B. Baker, Therapeutic strategies for enhancing angiogenesis in wound healing, Adv. Drug Deliv. Rev. 146 (2019) 97–125, https://doi.org/10.1016/j.addr.2018.09.010.
[6] G.A. James, E. Swogger, R. Wolcott, Ed Pulcini, P. Secor, J. Sestrich, J. W. Costerton, P.S. Stewart, Biofilms in chronic wounds, Wound Repair Regen. Off. Publ. Wound Heal. Soc. Eur. Tissue Repair Soc. 16 (2008) 37–44, https://doi.org/10.1111/j.1524-475x.2007.00321.x.
[7] P. Krzyszczyk, R. Schloss, A. Palmer, F. Berthiaume, The role of macrophages in acute and chronic wound healing and interventions to promote pro-wound healing phenotypes, Front. Physiol. 9 (2018) 419, https://doi.org/10.3389/fphys.2018.00419.
[8] L. Parisi, E. Gini, D. Baci, M. Tremolati, M. Fanuli, B. Bassani, G. Farronato, A. Bruno, L. Mortara, Macrophage polarization in chronic inflammatory diseases: killers or builders? J. Immunol. Res. 2018 (2018) 8917804 https://doi.org/10.1155/2018/8917804.
[9] H. Alkhoury, A. Hautmann, F. Erdmann, G. Zhou, S. Stojanović, S. Najman, T. Groth, Study on the potential mechanism of anti-inflammatory activity of covalently immobilized hyaluronan and heparin, J. Biomed. Mater. Res. Part A 108 (2020) 1099–1111, https://doi.org/10.1002/jbm.a.36885.
[10] F.O. Martinez, S. Gordon, The M1 and M2 paradigm of macrophage activation, F1000prime Rep. 6 (2014) 13, https://doi.org/10.12703/P6-13.
[11] H. Sorg, D.J. Tilkorn, S. Hager, J. Hauser, U. Mirastschijski, Skin wound healing: an update on the current knowledge and concepts, European surgical research. Europaische chirurgische Forschung, Rech. Chir. Eur. 58 (2017) 81–94, https://doi.org/10.1159/000454919.
[12] H. Roehrs, J.G.D. Stocco, F. Pott, G. Blanc, K. Crozeta, M.J. Meier, F.A.L. Dias, Dressings and topical agents containing hyaluronic acid for chronic wound healing, Cochrane Database of Systematic Reviews. https://doi.org/10.1002/14651858.CD012215.
[13] A.S. Asran, K. Razghandi, N. Aggarwal, G.H. Michler, T. Groth, Nanofibers from blends of polyvinyl alcohol and polyhydroxy butyrate as potential scaffold material for tissue engineering of skin, Biomacromolecules 11 (2010) 3413–3421, https://doi.org/10.1021/bm100912v.
[14] L.E. Tracy, R.A. Minasian, E.J. Caterson, Extracellular Matrix and Dermal Fibroblast Function in the Healing Wound, Adv. Wound care 5 (2016) 119–136, https://doi.org/10.1089/wound.2014.0561.
[15] S. Dhivya, V.V. Padma, E. Santhini, Wound dressings - a review, BioMedicine 5 (2015) 22, https://doi.org/10.7603/s40681-015-0022-9.
[16] G. Han, R. Ceilley, Chronic wound healing: a review of current management and treatments, Adv. Ther. 34 (2017) 599–610, https://doi.org/10.1007/s12325-017-0478-y.

[17] M. Hosseini, A. Shafiee, Engineering Bioactive Scaffolds for Skin Regeneration, Small 17 (2021) e2101384, https://doi.org/10.1002/smll.202101384.
[18] Y. Liu, T. Li, Y. Han, F. Li, Y. Liu, Recent development of electrospun wound dressing, Curr. Opin. Biomed. Eng. 17 (2021) 100247, https://doi.org/10.1016/j.cobme.2020.100247.
[19] C.-Y. Huang, K.-H. Hu, Z.-H. Wei, Comparison of cell behavior on pva/pva-gelatin electrospun nanofibers with random and aligned configuration, Sci. Rep. 6 (2016) 37960, https://doi.org/10.1038/srep37960.
[20] J. Shi, L. Wang, F. Zhang, H. Li, L. Lei, L. Liu, Y. Chen, Incorporating protein gradient into electrospun nanofibers as scaffolds for tissue engineering, ACS Appl. Mater. Interfaces 2 (2010) 1025–1030, https://doi.org/10.1021/am9007962.
[21] I. Lukin, I. Erezuma, L. Maeso, J. Zarate, M.F. Desimone, T.H. Al-Tel, A. Dolatshahi-Pirouz, G. Orive, Progress in Gelatin as Biomaterial for Tissue Engineering, Pharmaceutics 14 (2022), https://doi.org/10.3390/pharmaceutics14061177.
[22] N. Davidenko, C.F. Schuster, D.V. Bax, R.W. Farndale, S. Hamaia, S.M. Best, R. E. Cameron, Evaluation of cell binding to collagen and gelatin: a study of the effect of 2D and 3D architecture and surface chemistry, J. Mater. Sci. Mater. Med. 27 (2016) 148, https://doi.org/10.1007/s10856-016-5763-9.
[23] S. Zhang, Y. Huang, X. Yang, F. Mei, Q. Ma, G. Chen, S. Ryu, X. Deng, Gelatin nanofibrous membrane fabricated by electrospinning of aqueous gelatin solution for guided tissue regeneration, J. Biomed. Mater. Res. Part A 90 (2009) 671–679, https://doi.org/10.1002/jbm.a.32136.
[24] A. Ehrmann, Non-toxic crosslinking of electrospun gelatin nanofibers for tissue engineering and biomedicine-a review, Polymers 13 (2021), https://doi.org/10.3390/polym13121973.
[25] G. Decher, Fuzzy nanoassemblies: toward layered polymeric multicomposites, Science 277 (1997) 1232–1237, https://doi.org/10.1126/science.277.5330.1232.
[26] G. Apte, A. Repanas, C. Willems, A. Mujtaba, C.E.H. Schmelzer, A. Raichur, F. Syrowatka, T. Groth, Effect of different crosslinking strategies on physical properties and biocompatibility of freestanding multilayer films made of alginate and chitosan, Macromol. Biosci. 19 (2019) e1900181, https://doi.org/10.1002/mabi.201900181.
[27] A.S. Ivanov, L.V. Pershina, K.G. Nikolaev, E.V. Skorb, Recent progress of layer-by-layer assembly, free-standing film and hydrogel based on polyelectrolytes, Macromol. Biosci. 21 (2021) e2100117, https://doi.org/10.1002/mabi.202100117.
[28] C. Correia, R.O. Sousa, A.C. Vale, D. Peixoto, T.H. Silva, R.L. Reis, I. Pashkuleva, N. M. Alves, Adhesive and biodegradable membranes made of sustainable catechol-functionalized marine collagen and chitosan, Colloids Surf. B, Biointerfaces 213 (2022) 112409, https://doi.org/10.1016/j.colsurfb.2022.112409.
[29] J.M. Silva, A.R.C. Duarte, S.G. Caridade, C. Picart, R.L. Reis, J.F. Mano, Tailored freestanding multilayered membranes based on chitosan and alginate, Biomacromolecules 15 (2014) 3817–3826, https://doi.org/10.1021/bm501156v.
[30] A. Hautmann, D. Kedilaya, S. Stojanović, M. Radenković, C.K. Marx, S. Najman, M. Pietzsch, J.F. Mano, T. Groth, Free-standing multilayer films as growth factor reservoirs for future wound dressing applications, Biomater. Adv. 142 (2022) 213166, https://doi.org/10.1016/j.bioadv.2022.213166.
[31] S. Amorim, I. Pashkuleva, C.A. Reis, R.L. Reis, R.A. Pires, Tunable layer-by-layer films containing hyaluronic acid and their interactions with CD44, J. Mater. Chem. B 8 (2020) 3880–3885, https://doi.org/10.1039/D0TB00407C.
[32] A. Izquierdo, S.S. Ono, J.-C. Voegel, P. Schaaf, G. Decher, Dipping versus spraying: exploring the deposition conditions for speeding up layer-by-layer assembly, Langmuir 21 (2005) 7558–7567, https://doi.org/10.1021/la047407s.
[33] G. Cado, H. Kerdjoudj, A. Chassepot, M. Lefort, K. Benmlih, J. Hemmerlé, J.-C. Voegel, L. Jierry, P. Schaaf, Y. Frère, F. Boulmedais, Polysaccharide films built by simultaneous or alternate spray: a rapid way to engineer biomaterial surfaces, Langmuir ACS J. Surf. Colloids 28 (2012) 8470–8478, https://doi.org/10.1021/la300563s.
[34] I.P. Monteiro, A. Shukla, A.P. Marques, R.L. Reis, P.T. Hammond, Spray-assisted layer-by-layer assembly on hyaluronic acid scaffolds for skin tissue engineering, J. Biomed. Mater. Res. Part A 103 (2015) 330–340, https://doi.org/10.1002/jbm.a.35178.
[35] S.G. Caridade, C. Monge, F. Gilde, T. Boudou, J.F. Mano, C. Picart, Free-standing polyelectrolyte membranes made of chitosan and alginate, Biomacromolecules 14 (2013) 1653–1660, https://doi.org/10.1021/bm400314s.
[36] K. Cai, A. Rechtenbach, J. Hao, J. Bossert, K.D. Jandt, Polysaccharide-protein surface modification of titanium via a layer-by-layer technique: characterization and cell behaviour aspects, Biomaterials 26 (2005) 5960–5971, https://doi.org/10.1016/j.biomaterials.2005.03.020.
[37] S. Zankovych, J. Bossert, M. Faucon, U. Finger, K.D. Jandt, Selectively promoting or preventing osteoblast growth on titanium functionalized with polyelectrolyte multilayers, Adv. Eng. Mater. 13 (2011) B454–B461, https://doi.org/10.1002/adem.201180020.
[38] B.A. Aderibigbe, B. Buyana, Alginate in Wound Dressings, Pharmaceutics 10 (2018) 42, https://doi.org/10.3390/pharmaceutics10020042.
[39] S. Ahmed, S. Ikram, Chitosan based scaffolds and their applications in wound healing, Achiev. Life Sci. 10 (2016) 27–37, https://doi.org/10.1016/j.als.2016.04.001.
[40] J.S. Frenkel, The role of hyaluronan in wound healing, Int. Wound J. 11 (2014) 159–163, https://doi.org/10.1111/j.1742-481X.2012.01057.x.
[41] A. Köwitsch, G. Zhou, T. Groth, Medical application of glycosaminoglycans: a review, J. Tissue Eng. Regen. Med. 12 (2018) e23–e41, https://doi.org/10.1002/term.2398.
[42] H. Alkhoury, A. Hautmann, B. Fuhrmann, F. Syrowatka, F. Erdmann, G. Zhou, S. Stojanović, S. Najman, T. Groth, Studies on the mechanisms of anti-inflammatory activity of heparin- and hyaluronan-containing multilayer coatings-targeting NF-κB signalling pathway, Int. J. Mol. Sci. 21 (2020), https://doi.org/10.3390/ijms21103724.
[43] R. Altman, A. Bedi, A. Manjoo, F. Niazi, P. Shaw, P. Mease, Anti-inflammatory effects of intra-articular hyaluronic acid: a systematic review, Cartilage 10 (2019) 43–52, https://doi.org/10.1177/1947603517749919.
[44] M. Wu, Y. Du, Y. Liu, Y. He, C. Yang, W. Wang, F. Gao, Low molecular weight hyaluronan induces lymphangiogenesis through LYVE-1-mediated signaling pathways, PloS One 9 (2014) e92857, https://doi.org/10.1371/journal.pone.0092857.
[45] M. Muhammad, C. Willems, J. Rodríguez-Fernández, G. Gallego-Ferrer, T. Groth, Synthesis and Characterization of Oxidized Polysaccharides for In Situ Forming Hydrogels, Biomolecules 10 (2020), https://doi.org/10.3390/biom10081185.
[46] C. Santos de Oliveira, A.T. González, T. Hedtke, T. Kürbitz, A. Heilmann, C.E. H. Schmelzer, J. Martins de, S.E. Silva, Direct three-dimensional imaging for morphological analysis of electrospun fibers with laboratory-based Zernike X-ray phase-contrast computed tomography, Mater. Sci. Eng. C., Mater. Biol. Appl. 115 (2020) 111045, https://doi.org/10.1016/j.msec.2020.111045.
[47] S. Bolte, F.P. Cordelières, A guided tour into subcellular colocalization analysis in light microscopy, J. Microsc. 224 (2006) 213–232, https://doi.org/10.1111/j.1365-2818.2006.01706.x.
[48] Y. Jia, J. Li, Molecular assembly of Schiff Base interactions: construction and application, Chem. Rev. 115 (2015) 1597–1621, https://doi.org/10.1021/cr400559g.
[49] M. Zhao, L. Li, C. Zhou, F. Heyroth, B. Fuhrmann, K. Maeder, T. Groth, Improved stability and cell response by intrinsic cross-linking of multilayers from collagen I and oxidized glycosaminoglycans, Biomacromolecules 15 (2014) 4272–4280, https://doi.org/10.1021/bm501286f.
[50] C. Porcel, P. Lavalle, G. Decher, B. Senger, J.-C. Voegel, P. Schaaf, Influence of the polyelectrolyte molecular weight on exponentially growing multilayer films in the linear regime, Langmuir ACS J. Surf. Colloids 23 (2007) 1898–1904, https://doi.org/10.1021/la062728k.
[51] J. Campbell, A.S. Vikulina, Layer-By-Layer Assemblies of Biopolymers: Build-Up, Mechanical Stability and Molecular Dynamics, Polymers 12 (2020), https://doi.org/10.3390/polym12091949.
[52] C. Porcel, P. Lavalle, V. Ball, G. Decher, B. Senger, J.-C. Voegel, P. Schaaf, From exponential to linear growth in polyelectrolyte multilayers, Langmuir ACS J. Surf. Colloids 22 (2006) 4376–4383, https://doi.org/10.1021/la053218d.
[53] K.C. Krogman, J.L. Lowery, N.S. Zacharia, G.C. Rutledge, P.T. Hammond, Spraying asymmetry into functional membranes layer-by-layer, Nat. Mater. 8 (2009) 512–518, https://doi.org/10.1038/nmat2430.
[54] D. Volodkin, R. von Klitzing, Competing mechanisms in polyelectrolyte multilayer formation and swelling: Polycation–polyanion pairing vs. polyelectrolyte–ion pairing, Curr. Opin. Colloid Interface Sci. 19 (2014) 25–31, https://doi.org/10.1016/j.cocis.2014.01.001.
[55] J.J. Elsner, A. Shefy-Peleg, M. Zilberman, Novel biodegradable composite wound dressings with controlled release of antibiotics: microstructure, mechanical and physical properties, J. Biomed. Mater. Res. Part B, Appl. Biomater. 93 (2010) 425–435, https://doi.org/10.1002/jbm.b.31599.
[56] J. Kuchinka, C. Willems, D.V. Telyshev, T. Groth, Control of Blood Coagulation by Hemocompatible Material Surfaces-A Review, Bioeng. (Basel, Switz.) 8 (2021), https://doi.org/10.3390/bioengineering8120215.
[57] M. Zhao, G. Altankov, U. Grabiec, M. Bennett, M. Salmeron-Sanchez, F. Dehghani, T. Groth, Molecular composition of GAG-collagen I multilayers affects remodeling of terminal layers and osteogenic differentiation of adipose-derived stem cells, Acta Biomater. 41 (2016) 86–99, https://doi.org/10.1016/j.actbio.2016.05.023.
[58] G. Zhou, H. Loppnow, T. Groth, A macrophage/fibroblast co-culture system using a cell migration chamber to study inflammatory effects of biomaterials, Acta Biomater. 26 (2015) 54–63, https://doi.org/10.1016/j.actbio.2015.08.020.
[59] R. Sridharan, A.R. Cameron, D.J. Kelly, C.J. Kearney, F.J. O'Brien, Biomaterial based modulation of macrophage polarization: a review and suggested design principles, Mater. Today 18 (2015) 313–325, https://doi.org/10.1016/j.mattod.2015.01.019.
[60] G. Zhou, A. Liedmann, C. Chatterjee, T. Groth, In vitro study of the host responses to model biomaterials via a fibroblast/macrophage co-culture system, Biomater. Sci. 5 (2016) 141–152, https://doi.org/10.1039/c6bm00247a.
[61] J.E. Rayahin, R.A. Gemeinhart, Activation of Macrophages in Response to Biomaterials, in: M. Kloc (Ed.), Macrophages: Origin, Functions and Biointervention, Springer International Publishing, Cham, 2017, pp. 317–351.
[62] M. Saraiva, A. O'Garra, The regulation of IL-10 production by immune cells, Nature reviews, in: Immunology, 10, 2010, pp. 170–181, https://doi.org/10.1038/nri2711.
[63] H. He, S. Zhang, S. Tighe, J. Son, S.C.G. Tseng, Immobilized heavy chain-hyaluronic acid polarizes lipopolysaccharide-activated macrophages toward M2 phenotype, J. Biol. Chem. 288 (2013) 25792–25803, https://doi.org/10.1074/jbc.M113.479584.
[64] K.V. Eaton, H.L. Yang, C.M. Giachelli, M. Scatena, Engineering macrophages to control the inflammatory response and angiogenesis, Exp. Cell Res. 339 (2015) 300–309, https://doi.org/10.1016/j.yexcr.2015.11.021.
[65] J.E. Rayahin, J.S. Buhrman, Y. Zhang, T.J. Koh, R.A. Gemeinhart, High and low molecular weight hyaluronic acid differentially influence macrophage activation, ACS Biomater. Sci. Eng. 1 (2015) 481–493, https://doi.org/10.1021/acsbiomaterials.5b00181.